Water Oxidation

DOI: 10.1002/anie.201005141

Structural Modifications of Mononuclear Ruthenium Complexes: A Combined Experimental and Theoretical Study on the Kinetics of Ruthenium-Catalyzed Water Oxidation**

Lianpeng Tong, Lele Duan, Yunhua Xu, Timofei Privalov, and Licheng Sun**

Practical-efficiency catalysis of the water oxidation process ($2H_2O \rightarrow O_2 + 4e^- + 4H^+$) is the highly sought element of emerging artificial photosynthetic energy-conversion technology.[1,2] While oxygen evolution in naturally occurring photosynthesis, which supports nearly all existing life forms, relies on a sophisticated Mn-based complex,[1a,3] the majority of artificial molecular water-oxidation catalysts (WOCs) are Ru-based complexes with relatively simple polypyridyl ligands.[4,5]

Recently emerged evidence in favor of alternative O_2-evolving mechanisms for Ru-catalyzed water oxidation,[5] such as solvent water nucleophilic attack (WNA) and direct O–O coupling via interaction of two M–O units (I2M),[5a,6–8] demonstrated dramatic mechanistic consequences of different ligand designs, which are yet to be fully rationalized. Understanding of intricate ligand-dependent preferences for one mechanism over the other is necessary for further progress to be made.[5,7] Unfortunately, vast structural differences between Ru-bound ligands of WOCs which operate by the WNA or I2M mechanism hampers determinations of ligand influence on catalytic pathways.[5a]

Herein we report the synthesis of monomeric ruthenium complexes $[Ru^{II}(pda)L_2]$ (H_2pda: 1,10-phenanthroline-2,9-dicarboxylic acid; L is pyridine (py) in **1a**, 4-picoline (pic) in **1b**, or 4-bromopyridine in **1c**), which led us to the unprecedented discovery that a small alteration of a Ru-bound ligand, that is, replacement of 2,2′-bipyridine-6,6′-dicarboxylate (bda)[8] with pda, changes Ce^{IV}-driven catalytic water oxidation from a binuclear to a mononuclear process. Our experimental work, combined with a theoretical modeling study, shed light on the reaction intermediates and provided insight into the reaction pathways.

The crucial coordination features of previously reported $[Ru^{II}(bda)(pic)_2]$ (**2**) are 1) the large O-Ru-O cleft, which allows straightforward access of a solvent water molecule to the Ru center, and 2) the flexible bipyridine backbone, which provides adaptability to the Ru–ligand matrix at various oxidation states of the complex.[8b] We also reported that the kinetics of Ce^{IV}-driven catalytic water oxidation at pH 1 is second-order in the complex and, more importantly, an uncommon seven-coordinate Ru^{IV}–(OH) dimeric intermediate was isolated and structurally characterized.[8b,9] On the basis of these findings we suggested a bimolecular catalytic mechanism through direct interaction of two highly oxidized Ru(bda)–O units, which was further rationalized by DFT calculations.[6a]

Given the above considerations, we decided to investigate whether changing from a flexible to a highly preorganized (i.e., rigid)[10] backbone in **2** would give any insight into the structure–mechanism relationship. Complexes **1a–c** were synthesized in a one-pot reaction by heating $[Ru(dmso)_4Cl_2]$ and H_2pda to reflux in the presence of 1,8-diazabicyclo-[5.4.0]undec-7-ene overnight, followed by addition of the corresponding 4-substituted pyridines. We derived structures of **1a–c** (Figure 1) from ^1H NMR, HRMS, and elemental analysis data.[11] Specifically, the ^1H NMR spectra of **1a–c** in CD_3OD show two doublets and one singlet in the range of $\delta =$ 8.1–8.5 ppm, assigned to the six protons of pda, and indicative of a C_{2v}-symmetric Ru^{II}–pda (equatorial) plane in **1a–c**.

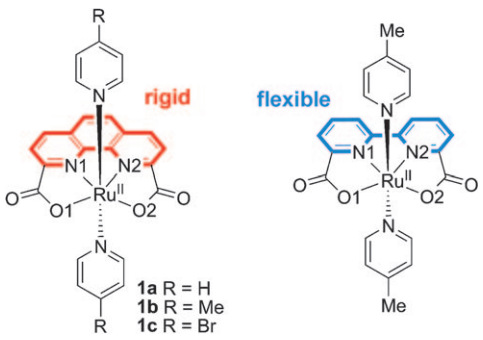

Figure 1. Molecular structures of **1a–c** and $[Ru^{II}(bda)(pic)_2]$ (**2**).

[*] L. Tong, L. Duan, Dr. Y. Xu, Prof. L. Sun
Department of Chemistry
School of Chemical Science and Engineering
Royal Institute of Technology (KTH), 10044 Stockholm (Sweden)
Fax: (+46) 8-791-2333
E-mail: lichengs@kth.se
Prof. L. Sun
State Key Laboratory of Fine Chemicals
DUT-KTH Joint Education and Research Center
on Molecular Devices
Dalian University of Technology (DUT), 116012 Dalian (China)
Prof. T. Privalov
Department of Organic Chemistry, Arrhenius Laboratory
Stockholm University, 10691 Stockholm (Sweden)
E-mail: priti@organ.su.se

[**] We thank the Swedish Research Council, the K & A Wallenberg Foundation, the Swedish Energy Agency, the China Scholarship Council (CSC), the National Science Foundation of China (20633020), and the National Basic Reseach Program of China (2009CB220009) for financial support of this work. We thank Dr. Guiling Zhao at Stockholm University for helping with MS measurements.

Supporting information for this article is available on the WWW under http://dx.doi.org/10.1002/anie.201005141.

At the B3LYP/lacvp** level of density functional theory,[12] which reproduced the X-ray crystal structure of **2** very well,[6a] we found that in isolated $[Ru^{II}(pda)L_2]$ complexes 1) pda is essentially planar;[13] 2) the Ru^{II}–pda (equatorial) plane is C_{2v}-symmetric; 3) the distance between the two oxygen donors O1 and O2 is about 0.2 Å shorter than that of an uncoordinated pda, and thus indicates bending distortions of carboxylate units on complexation (the reorganization energy[14] of pda due to complexation with Ru^{II} is ca. 31 kcal mol^{-1}); 4) the expanded O-Ru-O angle is larger than that of $[Ru^{II}(bda)(pic)_2]$ (ca. 130.5° versus ca. 124.7°, respectively).[15]

Studies on catalytic O_2 evolution with **1a–c** were carried out by using Ce^{IV} as oxidant ($2H_2O + 4Ce^{4+} \rightarrow O_2 + 4H^+ + 4Ce^{3+}$). In these experiments, the amount of evolved O_2 was monitored with an optical oxygen probe and verified by GC end-point reading. After six hours of catalytic reaction, turnover numbers (TONs) of 336, 310, and 190 were obtained for **1a**, **1b**, and **1c**, respectively. Based on the plots of O_2 evolution in the interval of 0–3600 s, we obtained initial turnover frequencies (TOFs) of 0.092, 0.102, and 0.040 s^{-1} for **1a**, **1b**, and **1c**, respectively. In comparison with molecular ruthenium catalysts reported by others,[4] **1a–c** are highly efficient. Specifically, **1a–c** show much better catalytic stability than their $[Ru^{II}(bda)(pic)_2]$ analogue **2**, which achieved a high TON of 1200 and a high initial TOF of 4.5 s^{-1} under the same experimental conditions but lost its catalytic activity over about 5 min.[16]

Besides diverse catalytic performance of **1a–c** relative to **2**, we discovered that kinetics of catalytic water oxidation for **1a–c** is clearly different from that of **2**. A kinetic study showed that the initial O_2 evolution rate for **1a–c** under catalytic conditions is first-order in catalyst concentration, as shown in Figure 2 for the case of **1b**. This indicates that a mononuclear catalytic process is involved in the rate-determining step of water oxidation by **1a–c**, contrary to the indication of a binuclear catalytic process for **2** under the same conditions.[8b] This experimental result reveals that a small change in ligand makes a big difference to the catalytic pathway. Additionally, the reaction kinetics proved to be zero-order in Ce^{IV} concentration (Figure S11 in the Supporting Information).

Investigation of the electrochemical properties of **1a–c** in aqueous CF_3SO_3H solution (pH 1.0) and phosphate-buffered saline (50 mM, pH 7.0) with $[Ru(bpy)_3Cl_2]$ (bpy: 2,2′-bipyridine) as external reference ($E_{1/2}(Ru^{II}/Ru^{III}) = 1.26$ V vs. NHE[17]), revealed that for all three Ru complexes the electrocatalytic water-oxidation onset potentials (ca. 1.55–1.65 V vs. NHE in pH 1.0 medium and ca. 1.23 V vs. NHE in pH 7.0 buffer) appeared at more anodic positions than the two preceding waves assigned to Ru^{III}/Ru^{IV} and Ru^{II}/Ru^{III}, respectively. For instance, the cyclic voltammogram (CV) of **1b** displays a quasireversible wave at $E_{1/2} = 0.97$ V (Ru^{II}/Ru^{III}) and an irreversible wave at $E = 1.36$ V (Ru^{III}/Ru^{IV}) in pH 1.0 medium (Figure S7), while the corresponding redox values for its Ru^{II}/Ru^{III} and Ru^{III}/Ru^{IV} couples in pH 7.0 buffer appear at $E = 0.82$ V and $E = 1.14$ V respectively (Figure S8; all potentials above are given in volts vs. NHE[18]). The previously reported CV of $[Ru^{II}(bda)(pic)_2]$ also featured clearly separated Ru^{II}/Ru^{III} and Ru^{III}/Ru^{IV} waves prior to the emergence of the water-oxidation onset at about 1.55 V,[8] and are qualitatively similar to the CV of **1b**.

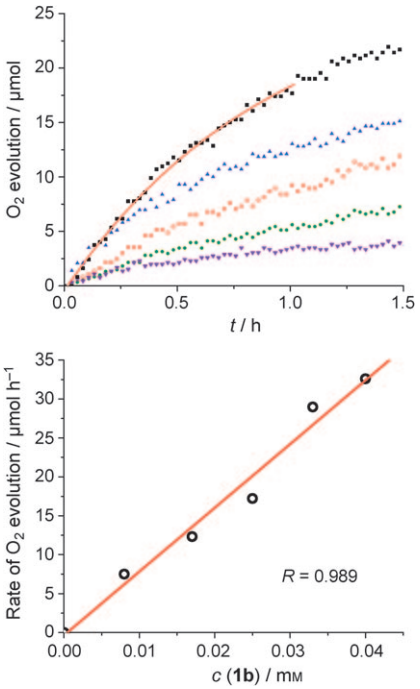

Figure 2. Upper: plots of O_2 evolution versus time at various concentrations of catalyst **1b**: 0.04 mM (■), 0.033 mM (▲), 0.025 mM (○), 0.017 mM (●), and 0.008 mM (▼). Lower: initial rate of O_2 evolution at various concentrations of catalyst **1b**, $k = 0.82$ L h^{-1}. A single exponential function was used to fit the generated dioxygen versus time plots during the period of 0–1 h (red curve, left); initial rate is calculated as the slope of the curve at $t = 0$.

With its advantageously low catalytic overpotential, **1a–1c** can achieve visible-light-driven water oxidation in neutral medium with $[Ru(bpy)_3]^{2+}$ as photosensitizer and $S_2O_8^{2-}$ as electron accepter (see the Supporting Information for details).

In our earlier study, HRMS allowed direct detection of relatively stable intermediates involved in water oxidation by **2**.[8] Employing a similar HRMS technique, we observed that in water containing 10% acetonitrile 1) the peak of $[Ru^{II}(pda)(pic)_2+H]^+$ was the only major signal for starting complex **1b**; 2) on addition of Ce^{IV} to the solution, signals of $[Ru^{IV}(pda)(pic)_2+OH]^+$ and $[Ru^{III}(pda)(pic)_2]^+$ appeared. In our previous work, analogous HRMS signal of $[Ru^{IV}(bda)(pic)_2+OH]^+$ were correctly assigned to the seven-coordinate $[Ru^{IV}(bda)(pic)_2(OH)]^+$, as confirmed by the X-ray crystal structure of the seven-coordinate $Ru^{IV}(OH)$ dimer.[8,9] Likewise, taking into account the similarly large O-Ru-O angle, we assigned the signal of the singly positively charged OH adduct to the seven-coordinate complex with Ru^{IV}-bound OH group, $[Ru^{IV}(pda)(pic)_2(OH)]^+$ (Figure 3).

To learn more about mechanistic aspects, we performed DFT modeling at the B3LYP/lacvp** level in water within a self-consistent polarizable continuum model;[12] electronic structure analysis was performed by using Mulliken atomic spin densities and natural bond orbital (NBO) analysis (see

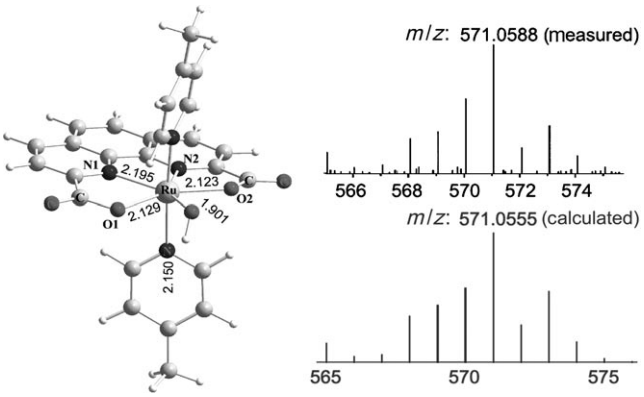

Figure 3. HRMS spectra assigned to $[Ru^{IV}(pda)(pic)_2(OH)]^+$: measured isotopic distribution (top right) and the calculated isotopic distribution (bottom right). DFT-optimized structure of $[Ru^{IV}(pda)(pic)_2(OH)]^+$ with all distances in angstrom (left).

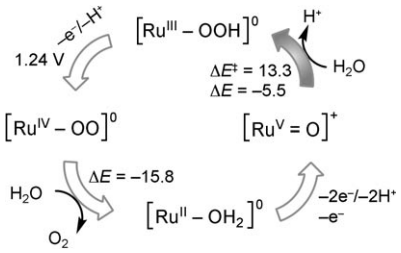

Scheme 1. Calculated O_2-evolution pathway by WNA. $\Delta E^{\ddagger}$ and ΔE are in kcal mol^{-1}, the redox potential of Ru^{III}-OOH is in volts versus NHE.

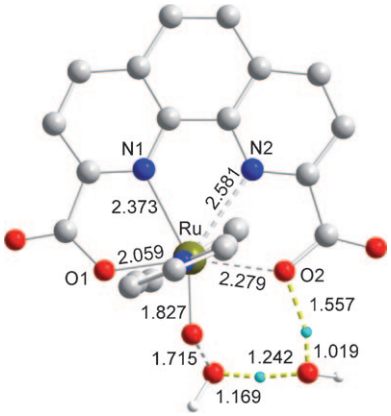

Figure 4. A WNA TS for formal complex $[Ru^V(pda)(py)_2{=}O]^+$. All bond lengths are in angstroms.

complete account of computational methods in the Supporting Information).[12]

Based on combined results of HRMS and electrochemical measurements we devised a sequence of proton-coupled oxidations: $[Ru^{III}{-}OH_2]^+ \rightarrow [Ru^{IV}{-}OH]^+ \rightarrow$formally $[Ru^V{=}O]^+$.[3,5] The calculated potentials for the formally Ru^{IV}/Ru^V and Ru^{III}/Ru^{IV} proton-coupled oxidation steps are 1.67 V versus NHE and 1.28 V versus NHE, respectively,[19,20] consistent with electrochemical measurements.

Geometries of the above-mentioned aqueous complexes, results of our earlier work,[6a] and calculated ligand reorganization energies ΔE_L(pda) and ΔE_L(bda) (Table 1)[14,21] highlighted the disparity between pda and bda ligands. Combined torsion of the bipyridine backbone and O1-Ru-O2/N1-Ru-N2 planes adjusts bda to the positive charge (ionic radius) of the ruthenium ion. This adjustability is mirrored by the variation of ΔE_L(bda), which is at maximum for the "high-stress" $[Ru^{IV}{-}OH]^+$ complex with about 10° twist of the bipyridine backbone and about 23° torsion between O-Ru-O and N-Ru-N planes.[22] Conversely, the rigidity of pda leaves very little room for adaptability, as mirrored by a fairly constant ΔE_L(pda), although there is a clear mismatch between ionic radii of $Ru^{III/IV}$ (ca. 0.65–0.62 Å) and the selectivity of pda towards larger metal ions (ca. 1.0 Å).[23]

Table 1: Calculated ligand reorganization energies [kcal mol^{-1}].[a]

	ΔE_L(pda)	ΔE_L(bda)
$[Ru^{III}{-}OH_2]^+$	32	26
$[Ru^{IV}{-}OH]^+$	34	36
$[Ru^V{=}O]^+$	34	27

[a] All values for ΔE_L were calculated at the B3LYP/6-31g**++ level of theory.

To get an idea about the potential-energy profiles of O_2 evolution catalyzed by **1b**, we proceeded with modeling of plausible mononuclear pathway (WNA) with attack on formal complex $[Ru^V(pda){=}O]^+$ proceeding with proton-coupled reduction, formally $Ru^V \rightarrow Ru^{III}$ (Scheme 1).[24] O–O bond formation is exothermic ($\Delta E = -5.5$ kcal mol^{-1}); the electronic energy barrier $\Delta E^{\ddagger}$ is 13.3 kcal mol^{-1}. In the properly characterized transition state (TS, Figure 4), the proton-accepting relay involves *syn* lone pairs of one of COO^- groups.[25] This finding is reminiscent of 1) the acid–base proton relay in bleomycins,[26] and 2) involvement of aspartate-COO^- in the naturally occurring oxygen-evolving complex.[3] The "shift" of Ru^{III} occurs at the TS (see Figure 4), because the cleft of pda is both rigid and too large for the ionic radius of Ru^{III}.[27] It is therefore intuitively reasonable that auxiliary COO^- group participates in a proton reshuffle. For the analogous WNA on formal complex $[Ru^V(bda){=}O]^+$, the "shift" of Ru^{III} inside the cleft of bda occurs, too, but to a lesser extent (Figure S15). For comparison, the barrier for O–O bond formation by WNA on $[Ru^V(bda){=}O]^+$ is 18 kcal mol^{-1}. The higher barrier indicates that **2** does not go through the WNA pathway as easily as **1b**.

The ligand–metal coordination in TS (WNA) in Figure 4 is similar to that in weakly bound seven-coordinate complex $[Ru^{III}(pda)(OH_2)]^+$ (Figure S14A), in which the "shift" of Ru^{III} inside pda occurs for the reasons detailed above. On the contrary, we found no such asymmetry in the analogous aqua Ru^{III}(bda) complex.[6a] Furthermore, the "shift" of the Ru^V unit, combined with ligand reorganization, in the preceding $[Ru^V(pda){=}O]^+$ complexes requires less energy in comparison with $[Ru^V(bda^{2-}){=}O]^+$ (Figure S20). On the basis of these results, we suggest that the smaller WNA barrier of **1b** (Table 2) is related to lower overall reorganization energy of

Table 2: Calculated O–O bond formation barriers [kcal mol^{-1}] in water.

	$[Ru^{V}(pda)(py)_2{=}O]^{+}$	$[Ru^{V}(bda)(py)_2{=}O]^{+}$
SWNA	13.3[a]	18.0[a]
$Ru^{V}{=}O$ coupling	16.4[a]	11.9[b]

[a] Present work. [b] Reference [6a].

forming the TS, whereas the adjustability of bda could inhibit reorganization of **2** towards the Ru^{III} TS (Figure S15) in the WNA process. The disparity of the ligand reorganization energies (Table 1) is additional support for our view of the plausible cause of the mechanistic selectivity.

Proton-coupled one-electron oxidation of aqueous Ru^{III}–OOH (calcd 1.24 V vs. NHE) leads to formal peroxo complex Ru^{IV}–OO (this oxidative step is unlikely to be rate-limiting due to the very large excess of the oxidant). The subsequent displacement of O_2 by a solvent water molecule has substantial driving force ($\Delta E = -15.8$ kcal mol^{-1}). The ground electronic state of the peroxo complex is a triplet: one unpaired electron is localized on ruthenium and one electron is delocalized over the OO moiety. Remarkably, properties of our Ru^{IV}–OO peroxo complex are in line with those calculated by Van Voorhis and co-workers for comparable analogue $[Ru^{II}(tpy)(bpm)(OH_2)]^{2+}$.[6b]

We also checked the I2M pathway for **1b**, making use of the procedure described in our earlier study,[6a] and obtained a barrier of 16.4 kcal mol^{-1} (in water). Due to less torsion of O1-Ru-O2/N1-Ru-N2 planes (Table S7), increased collision of axial ligands hinders two formal (pda)Ru^{V}=O species getting close and thus increases the barrier for their direct O–O coupling in comparison to the coupling of two formal (bda)Ru^{V}=O species investigated in our earlier work.[6a]

In summary, we have discovered that a small alteration of an Ru^{II}-bound ligand, that is, replacement of 2,2′-bipyridine-6,6′-dicarboxylate (bda) with 1,10-phenanthroline-2,9-dicarboxylate (pda), changes Ce^{IV}-driven catalytic water oxidation from a binuclear to a mononuclear process. Combining the results of electrochemical and HRMS studies allowed us to propose that $[Ru^{III}(pda)(H_2O)]^{+}$ and $[Ru^{IV}(pda)(OH)]^{+}$ are involved in the process as intermediates. We compared two mechanisms by computational modeling—solvent water nucleophilic attack and direct O–O coupling for WOCs with pda and bda ligands—and obtained initial underpinning of the experimental observations. Qualitatively, our study for the first time suggests a link between a water oxidation pathway and different geometries of WOCs in catalytic states, which indicates that the torsional flexibility of bda, the rigidity of pda, and their reorganizations through the catalytic cycle are implicated. The modeling study also indicated that a dicarboxylate ligand may assist a proton-coupled nucleophilic attack towards monomeric Ru^{V}=O by preorienting the reactant water molecule and perhaps even promoting heterolytic cleavage of an O–H bond.[6b]

Our findings help to bring the ligand-dependent "borderline" between alternative catalytic pathways of water oxidation into a spotlight, so that it can become better understood, and stimulates design of more efficient catalysts for water oxidation.

Received: August 17, 2010
Revised: October 1, 2010
Published online: December 9, 2010

Keywords: density functional calculations · homogeneous catalysis · N,O ligands · ruthenium · water splitting

[1] a) J. Barber, *Chem. Soc. Rev.* **2009**, *38*, 185–196; b) X. Sala, I. Romero, M. Rodríuez, L. Escriche, A. Llobet, *Angew. Chem.* **2009**, *121*, 2882–2893; *Angew. Chem. Int. Ed.* **2009**, *48*, 2842–2852; c) J. H. Alstrum-Acevedo, M. K. Brennaman, T. J. Meyer, *Inorg. Chem.* **2005**, *44*, 6802–6827; d) J. K. Hurst, *Science* **2010**, *328*, 315–316.

[2] N. S. Lewis, D. G. Nocera, *Proc. Natl. Acad. Sci. USA* **2006**, *103*, 15729–15735.

[3] a) P. E. M. Siegbahn, *Acc. Chem. Res.* **2009**, *42*, 1871–1880; b) T. J. Meyer, M. H. V. Huynh, H. H. Thorp, *Angew. Chem.* **2007**, *119*, 5378–5399; *Angew. Chem. Int. Ed.* **2007**, *46*, 5284–5304.

[4] a) S. Masaoka, K. Sakai, *Chem. Lett.* **2009**, *38*, 182–183; b) Y. Xu, T. Åkermark, V. Gyollai, D. Zou, L. Eriksson, L. Duan, R. Zhang, B. Åkermark, L. Sun, *Inorg. Chem.* **2009**, *48*, 2717–2719; c) R. Zong, R. P. Thummel, *J. Am. Chem. Soc.* **2005**, *127*, 12802–12803; d) C. Sens, I. Romero, M. Rodriguez, A. Llobet, T. Parella, J. Benet-Buchholz, *J. Am. Chem. Soc.* **2004**, *126*, 7798–7799; e) T. J. Meyer, M. H. V. Huynh, *Inorg. Chem.* **2003**, *42*, 8140–8160.

[5] a) S. Romain, L. Vigara, A. Llobet, *Acc. Chem. Res.* **2009**, *42*, 1944–1953; b) J. J. Concepcion, J. W. Jurss, M. K. Brennaman, P. G. Hoertz, A. O. T. Patrocinio, N. Y. M. Iha, J. L. Templeton, T. J. Meyer, *Acc. Chem. Res.* **2009**, *42*, 1954–1965.

[6] a) J. Nyhlén, L. Duan, B. Åkermark, L. Sun, T. Privalov, *Angew. Chem.* **2010**, *122*, 1817–1821; *Angew. Chem. Int. Ed.* **2010**, *49*, 1773–1777; b) L.-P. Wang, Q. Wu, T. V. Voorhis, *Inorg. Chem.* **2010**, *49*, 4543–4553; c) X. Yang, M.-H. Baik, *J. Am. Chem. Soc.* **2008**, *130*, 16231–16240.

[7] a) L. Duan, Y. Xu, M. Gorlov, L. Tong, S. Andersson, L. Sun, *Chem. Eur. J.* **2010**, *16*, 4659–4668; b) D. J. Wasylenko, C. Ganesamoorthy, B. D. Koivisto, M. A. Henderson, C. P. Berlinguette, *Inorg. Chem.* **2010**, *49*, 2202–2209; c) M. Yoshida, S. Masaoka, K. Sakai, *Chem. Lett.* **2009**, *38*, 702–703.

[8] a) L. Duan, Y. Xu, P. Zhang, M. Wang, L. Sun, *Inorg. Chem.* **2010**, *49*, 209–215; b) L. Duan, A. Fischer, Y. Xu, L. Sun, *J. Am. Chem. Soc.* **2009**, *131*, 10397–10399.

[9] The overall structure of the seven-coordinate Ru^{IV} dimeric species is μ-(HOHOH)$[Ru^{IV}(bda)(pic)_2]_2(PF_6)_3{\cdot}2H_2O$.

[10] The ligand is said to be preorganized if its free form has the same conformation as is required to complex a metal ion. See also N. J. Williams, N. E. Dean, D. G. VanDerveer, R. C. Luckay, R. D. Hancock, *Inorg. Chem.* **2009**, *48*, 7853–7863, and references therein.

[11] In aqueous media mixed with acetonitrile, ^{1}H NMR revealed that **1a–c** are almost 100% coordinated with MeCN. The HRMS signal of $Ru^{II}(pda)L_2$–NCMe is nonetheless very weak relative to the signal of the six-coordinate $[Ru^{II}(pda)L_2]$ (see details in the Supporting Information). The same holds for $[Ru^{II}(bda)(pic)_2]$.

[12] All relevant references regarding the computational methods can be found in the Supporting Information.

[13] The auxiliary carboxylate groups share the delocalized electronic density with the π system and are therefore coplanar with the phenanthroline backbone even in free pda; see also D. L. Melton, D. G. VanDerveer, R. D. Hancock, *Inorg. Chem.* **2008**, *47*, 2000–2010.

[14] The difference between the minimized electronic energy of a free ligand and the electronic energy of the conformation a

ligand assumes in a Ru complex (single-point); see also the Supporting Information.
[15] In the X-ray crystal structure of **2**, the O1-Ru-O2 angle is 122.99°; the calculated value is very close to this value.[6a]
[16] L. Duan, L. Sun et al. unpublished results.
[17] H. Reiss, A. Heller, *J. Phys. Chem.* **1985**, *89*, 4207 – 4213.
[18] For clarity, we consider the formal oxidation states of Ru, taking into account the actual electron distribution (obtained by DFT) where necessary.
[19] a) M. H. Baik, R. A. Friesner, *J. Phys. Chem. A* **2002**, *106*, 7407 – 7412; b) L. E. Roy, E. Jakubikova, G. Guthrie, E. R. Batista, *J. Phys. Chem. A* **2009**, *113*, 6745 – 6750; c) S. Blasco, I. Demachy, Y. Jean, A. Lledos, *New J. Chem.* **2001**, *25*, 611 – 617.
[20] We made use of in-solvent Born–Haber cycle, as described in reference [19] and our earlier study.[6a] See details in the Supporting Information.
[21] For clarity of comparison with pda, ΔE_L(bda) was calculated with respect to free *cis*-bda.
[22] Calculated torsion angles are in agreement with those in the X-ray crystal structure of the seven-coordinate Ru^{IV}–OH dimeric intermediate from reference [8b].
[23] Already such metal ions as Cu^{II} (ionic radius of 0.73 Å) and Zn^{II} (ionic radius of 0.74 Å) are considered too small for pda; see reference [10].
[24] WNA mechanism for an Mn porphyrin model complex: a) T. Privalov, L. Sun, B. Åkermark, J. Liu, Y. Gao, M. Wang, *Inorg. Chem.* **2007**, *46*, 7075 – 7086; b) Y. Gao, T. Åkermark, J. Liu, L. Sun, B. Åkermark, *J. Am. Chem. Soc.* **2009**, *131*, 8726 – 8727.
[25] The normal vibrational mode associated with the single imaginary frequency exhibits proton-coupled formation of Ru^{III}–OOH. A scan of the intrinsic reaction coordinate proved connectivity of the WNA TS with proper near- and after-attack complexes.
[26] D. Kumar, H. Hirao, S. Shaik, P. M. Kozlowski, *J. Am. Chem. Soc.* **2006**, *128*, 16148 – 16158, and references therein.
[27] R. D. Shannon, *Acta Crystallogr. Sect. A* **1976**, *32*, 751 – 767.

